MicroRNA-19b regulates proliferation and differentiation along the medial-lateral axis of the developing avian pallium

Suvimal Kumar Sindhu, Archita Mishra[§], Niveda Udaykumar[§], Jonaki Sen*

Department of Biological Sciences & Bio-engineering,
Indian Institute of Technology Kanpur,
Kanpur-208016, UP, India

[§] Equal contribution

*Corresponding Author: jonaki@iitk.ac.in

Keywords**:** miR-19b, *Neurod1*, Chick, Forebrain, *Mef2c*, Mesopallium

Running title: miR-19b & medio-lateral biased proliferation & differentiation

Summary statement**:** miR-19b regulates proliferation and differentiation in the avian pallium

ABSTRACT

The avian and mammalian brain contain similar cell types, but are organized quite differently. The dynamic changes in proliferation and differentiation of neuronal progenitors along the medial-lateral axis are among the unique features that distinguish the avian pallium from its mammalian counterpart. In this study carried out in the developing chick pallium, the analysis of expression pattern as well as functional studies of a microRNA, miR-19b, reveal that it is a potential regulator of the dynamics of neuronal progenitor proliferation and neuronal differentiation in this context. Moreover, miR-19b was also found to be sufficient for regulating the expression of a lateral pallial marker, *Mef2c*. In summary, miR-19b is likely to be a pivotal player that shapes the developing avian pallium.

INTRODUCTION

The dorsal portion of the vertebrate forebrain is known as the pallium. Unlike the mammalian pallium which comprises of a highly organized and multilayered structure, the neocortex, the avian pallium contains several spatially segregated clusters of nuclei such as the dorso-medial (DM) cluster, the dorso-lateral (DL) cluster, the hyperpallium, the mesopallium, etc. (Briscoe et al., 2018; Dugas-Ford et al., 2012; Gupta et al., 2012; Suzuki et al., 2012). In the avian pallium, medial and lateral regions exhibit temporally-biased neurogenic differentiation (Gupta et al., 2012; Suzuki et al., 2012). In the medial pallium neuronal progenitor proliferation and differentiation ceases relatively earlier than in the lateral pallium (Gupta et al., 2012; Suzuki et al., 2012). Surprisingly, till date there is very limited information available about the mechanisms controlling neurogenesis in the avian pallium. Recently, a paired homeodomain-containing transcription factor, Pax6

which is expressed in the neural stem/progenitor cells throughout the medial and lateral pallium (Kawakami et al., 1997), is required for regulating the number of post-mitotic immature neurons in the chick forebrain (Yamashita et al., 2018). However, it remains to be discovered how the temporal difference in proliferation and differentiation between the medial and lateral avian pallium is achieved.

RESULTS & DISCUSSION

In a previous study, we have demonstrated that a microRNA, miR-19b is expressed in the neural stem/progenitor cells residing in the ventricular zone (VZ) throughout the medial and lateral pallium of the developing chick forebrain at Hamilton and Hamburger stage 24 (HH24) or embryonic day 4.5 (E4.5) (Hamburger and Hamilton, 1951; Sindhu et al., 2019) (Fig.1.A, D and M). Interestingly, further analysis at HH29 (E6.5) revealed that the expression of miR-19b is much lower in the VZ of the medial pallium as compared to that of the lateral pallium (Fig. 1E, E', E'', E'*, E''*, H, H' and H''). However, at HH35 (E8.5), miR-19b expression drops down to very low levels both in the VZ of the medial as well as the lateral pallium (Fig. 1I, I', I'',I'*, I''*, L, L' and L''). This is in contrast to the strong expression of miR-19b observed in the dorsal ventricular ridge (DVR) region at this stage (Fig. 1I, I', I'',I'*, I''*, L, L' and L''). In summary, the expression of miR-19b in the VZ of the pallium starts to decline along the media-lateral axis in a temporally regulated manner (Fig. 1A, E, I and M). Apart from the dynamic expression pattern observed in the chick forebrain, in mammals, miR-19b has been shown to regulate (a) the number of neural stem cells in the forebrain (Bian et al., 2013), and (b) the expression of Beta2/*Neurod1*, in pancreatic β-cells (Lee et al., 1995; Pataskar et al., 2016; Zhang et al., 2011). Hence,

based on all of the above we hypothesized that miR-19b is likely to be one of the key factors that regulate proliferation and differentiation of neuronal progenitors in the avian pallium and thereby contributing to patterning along the medial-lateral axis.

Before investigating the role of miR-19b in regulation of proliferation of neuronal progenitor cells in the avian pallium, we first compared the expression pattern of miR-19b with the location of phospho-histone 3 (PH3), a marker of cells in the M-phase of the cell-cycle. We found that cell proliferation in the VZ, represented by PH3 positive cells, exhibits medial-lateral dynamics spanning several stages of forebrain development, similar to that observed for the expression of miR-19b (Fig. 1B, B', F, F', F'', J, J', J'' and M). The presence of miR-19b and PH3 positive cells in similar tissue domains indicated that miR-19b is likely to promote proliferation in the avian pallium. This is additionally supported by a previous study reporting the ability of miR-19b to regulate neural stem cell number in the mouse forebrain (Bian et al., 2013).

In addition to regulating cell proliferation, we had hypothesized that miR-19b may also be involved in the regulation of neuronal differentiation, possibly through the inhibition of *Neurod1,* a neurogenic differentiation factor. To determine if this is true we compared the expression pattern of *Neurod1* and miR-19b in the developing chick forebrain. At HH24, miR-19b was found to be expressed throughout the medial and lateral VZ as mentioned above (Fig. 1A, A'), whereas *Neurod1*, was found to be expressed throughout the medial and lateral region in the sub-ventricular zone (SVZ) (Fig. 1C, C' and M). This indicated that miR-19b and *Neurod1* are expressed in mutually exclusive domains right after the

formation of the forebrain vesicles. At HH29, miR-19b started to decline in the medial region relative to lateral region whereas *Neurod1* was found to be expressed in the SVZ in the medial region alone (Fig. 1E, E', E'', G, G', G'', H, H' and H'' and Fig. S1B to E). At HH35, the expression of miR-19b decreased from VZ of the lateral region as well, while relatively high levels of *Neurod1* expression was observed in the SVZ of the lateral region (Fig. 1I, I', I'', I'*, I''*, K, K', K'', L, L' and L''). In summary, *Neurod1* was found to be expressed mostly in the post-mitotic immature neurons present in the SVZ at all the stages analyzed (Fig. 1C, C', G, G', G'', K, K' and K'' and Fig. S1C to E), whereas miR-19b is expressed mostly in the VZ at these stages (Fig. 1A, A', E, E', E'', I, I' and I'' and Fig. S1B and E). Thus miR-19b and *Neurod1* are expressed adjacent to each other, in mutually exclusive spatial domains (Fig. 1D, D', H, H', H'', L, L', L'', M and Fig. S1D and E), which is in keeping with the expression pattern exhibited by a microRNA and its target mRNA (Stark et al., 2005).

To investigate whether miR-19b functions as a regulator of cell proliferation of neuronal progenitors, we manipulated the expression of miR-19b in the developing chick forebrain, using the avian retrovirus RCASBP(A) (Petropoulos and Hughes, 1991). For gain-of-function experiments, GFP along with miR-19b was transduced using the RCAS-miR19b construct and as a control, GFP alone was transduced using the RCAS-GFP construct (Fig. 2A). We electroporated these constructs at HH22 and harvested and analyzed the lateral pallium at HH34, where some PH3 positive cells were present. We found that overexpression of miR-19b in the VZ of lateral pallium leads to an increase in cell proliferation as shown by a significant increase in the percentage of PH3-GFP double-

positive cells in comparison to the control (RCAS-GFP: 3.74 ± 0.21%, RCAS-miR-19b: 7.29 ± 0.8%; Fig. 2C, D and F). We also performed loss-of-function using a miRNA:Sponge named Sponge-19b, which is comprised of twelve copies of the miR-19b target sequence and is designed to sequester miR-19b (Ebert and Sharp, 2010) (Fig. S4A and B). Before this, we tested the ability of Sponge-19b to inhibit the function of miR-19b using an *in vitro* sensor assay (see materials and method). Once Sponge-19b was found to be effective through the *in vitro* assay, we used this construct for manipulation of miR-19b function *in vivo*. We used RCAS-Sponge-19b construct to transduce Sponge-19b in the VZ of lateral pallium at similar stages as mentioned above (Fig. 2A and B), upon analysis it was revealed that there is a significant decrease in percentage of PH3-GFP double-positive cells (RCAS-Sponge-19b: 2.06 ± 0.22%, RCAS-GFP: 3.74 ± 0.21%; Fig. 2C, E and F). These results demonstrate that miR-19b is both necessary and sufficient for regulating the number of PH3 positive cells. This supports our hypothesis that miR-19b is responsible for controlling cell proliferation in the developing avian pallium.

Based on the mutually exclusive expression domains of *Neurod1* and miR-19b as well as a report where *Neurod1* mRNA is shown to be regulated by miR-19b in the mouse pancreatic cells (Zhang et al., 2011), we decided to test whether miR-19b regulates the expression of *Neurod1* in the avian pallium as well. We began by studying the regulation of miR-19b and *Neurod1 in vitro*, for *which* we devised a sensor assay to determine if the chick *Neurod1* mRNA target region predicted by TargetScan (Agarwal et al., 2015), can interact with miR-19b (Fig. S2). A construct expressing GFP along with miR-19b (pRmiR-19b) (Smith et al., 2009) (Fig. S3A) was co-transfected with a construct referred to as

Sensor-ND1-WT, where the mCherry reporter is placed upstream of the chick *Neurod1* target region, into HEK 293T cells (Fig. S3A and B). This resulted in significant suppression of mCherry fluorescence as compared to the control (pRmiR-Empty with Sensor-ND1-WT: 15.66 ± 0.15 A.U., pRmiR-19b with Sensor-ND1-WT: 7.53 ± 0.03 A.U.; Fig. S3C-H and L). However, when pRmiR-19b was co-transfected with Sensor-ND1-MUT, a construct containing mutations in the miR-19b target region (Fig. S3A and B), the repression of mCherry expression was abolished (pRmiR-19b with Sensor-ND1-WT: 7.53 ± 0.03 A.U., pRmiR-19b with Sensor-ND1-MUT: 14.62 ± 0.24 A.U.; Fig. S3F to K and L). These results suggest that miR-19b can directly regulate *Neurod1* in a sequence-dependent manner *in vitro*.

To examine whether the *in vitro* interaction of miR-19b with *Neurod1* is a true reflection of a similar interaction in the developing chick forebrain, we carried out the following gain-of-function experiments. We electroporated RCAS-miR19b and as a control, RCAS-GFP constructs (Fig. 3A) at HH22 and harvested and analyzed the brains at HH34 (Fig. 3B). We found that in comparison to the control, misexpression of miR-19b in the SVZ significantly reduced the percentage of GFP-positive cells that are *Neurod1*-GFP double-positive (RCAS-GFP: 68.17 ± 0.89%, RCAS-miR-19b: 35.79 ± 7.85%; Fig. 3C to H and I). This indicated that miR-19b is sufficient for regulating the expression of *Neurod1* in the developing chick forebrain. For loss-of-function experiments with miR-19b, RCAS-Sponge-19b, and as a control, RCAS-GFP constructs were used at similar stages as mentioned above (Fig. S5A and B) and the VZ was analyzed, where miR-19b is enriched. Surprisingly, in the VZ there was no significant increase in the percentage of GFP-positive

cells that are *Neurod1*-GFP double-positive (RCAS-GFP: 10.24 ± 7.32%, RCAS-Sponge-19b: 13.52 ± 6.21%; Fig. S5C to H and I). This could be attributed to either the absence of other factors in the VZ necessary for *Neurod1* expression or to the presence of additional factors apart from miR-19b, which prevent *Neurod1* from being expressed in the VZ.

Since miR-19b and *Neurod1* together appear to control aspects of proliferation and differentiation in the developing chick forebrain, therefore we now wanted to determine if these molecular players could also contribute towards defining the identity of differentiating neurons, that are regionally segregated in the avian forebrain (Suzuki et al., 2012). *Mef2c* is expressed as early as HH29, in one of the large clusters of neurons located in the lateral region of the avian pallium known as the mesopallium (Suzuki et al., 2012). To test the effect of manipulating miR-19b on the expression of the mesopallium marker- *Mef2c*, we misexpressed miR-19b by electroporating pRmiR-19b and as a control, the pRmiR-Empty construct, at HH22 and harvested and analyzed the brains at HH29 (Fig. 4A and B). Since we were analyzing the brains at HH29, which is only 72hrs after electroporation, transient expression from the constructs would suffice, thus we decided to use pRmiR-based constructs instead of the RCAS-based constructs in this case. When we examined the region of the lateral pallium marked by GFP expression, where miR-19b was misexpressed, we observed a loss of expression of *Mef2c* within this region, (Fig. 4C to E). However, there was no change in the expression of *Mef2c* in the forebrain electroporated with pRmiR-Empty control (Fig. 4F to H). This indicated that miR-19b is sufficient for regulating the expression of *Mef2c* in the avian mesopallium.

Differentiating neurons in the mesopallium before expressing *Mef2c*, transiently express *Neurod1* when they are post-mitotic immature neurons (Gupta et al., 2012; Suzuki et al., 2012). Besides, we have shown that miR-19b is sufficient for repressing the expression of both *Neurod1* and *Mef2c*. Taking the above two facts into consideration we wanted to determine whether miR-19b mediated loss of expression of *Mef2c* in the mesopallium is dependent on loss of expression of *Neurod1*. For this, we electroporated at HH22 the pCAG-*Neurod1*-DBD-EnR construct that expresses a dominant-negative form of *Neurod1* (Yan and Wang, 2004) together with pCAG-GFP (for marking the electroporated region), and harvested and analyzed the brains at HH29 (Fig. 4A and B). Indeed, we found that the region expressing GFP showed loss of expression of *Mef2c* (Fig. 4I to K), suggesting that miR-19b mediated inhibition of *Mef2c* expression in the avian pallium, is likely to be due to inhibition of *Neurod1* expression.

Conclusions

In summary, we have discovered novel functions of miR-19b that contribute towards the medial-lateral patterning of the avian pallium. First, we found that miR-19b is expressed dynamically along the medial-lateral axis of the developing chick pallium. Further, we found that while the dynamics of expression of miR-19b mirrors the dynamics of the proliferating cells, it is mutually exclusive with the expression dynamics of *Neurod1*, a crucial regulator of neuronal differentiation. Experiments that functionally manipulate miR-19b strongly indicated that it is likely to be involved in promoting proliferation while at the same time it inhibits neuronal differentiation by regulating *Neurod1*. Moreover, miR-19b

also seems to be sufficient for regulating the expression of *Mef2c* a marker of the mesopallium region. Overall, this study sheds light on some of the molecular mechanisms that control the dynamics of neuron formation in the avian brain.

MATERIALS & METHODS

Animals (Fertilized chicken eggs)

Fertilized chicken eggs from the White Leghorn variety were purchased from Ganesh Enterprises, Nankari, Indian Institute of Technology Kanpur, Uttar Pradesh, India. These eggs were incubated in a humidified incubator at 38 ˚C until desired Hamilton Hamburger (HH) stages (Hamburger and Hamilton, 1951).

Cell culture

Human embryonic kidney (HEK-293T) cells were cultured with 10% Fetal Bovine Serum in Dulbecco's Modified Eagle's Medium (DMEM) media.

Tissue section preparation

The chick embryo at the desired HH stages were taken and brains were dissected out. The fixation was performed at 4˚C overnight in 4% Paraformaldehyde (PFA). These brains were washed with phosphate buffer saline (PBS), and then after dehydration was performed in 30% sucrose they were embedded in Polyfreeze (Sigma, P0091). Finally, a cryostat (Leica CM 1850) was used to obtain 12-16 µm thick sections of the chick pallium.

RNA *in situ* hybridization

For micro RNA *in situ* hybridization, a probe was designed where the 3'end of the antisense sequence of miR-19b was labeled with digoxigenin (Eurofins MWG Operon). This probe was used to perform section RNA *in situ* hybridization using a published protocol (Thompson et al., 2007). Finally, the detection was performed using another published method (Trimarchi et al., 2007).

The mRNA *in situ* hybridization was performed on the tissue sections using a published method (Trimarchi et al., 2007). The following cDNA clones were used to prepare probes: (1) pCRII-TA-*Mef2c* (gift from Prof. Tatsumi Hirata, National Institute of Genetics, Japan); (2) *Neurod1* (ChEST 695k11) obtained from Source Bioscience.

DNA constructs preparation

1. pRmiR-19b and RCAS-miR-19b: pRmiR-Empty construct (Smith et al., 2009) after BsaI digestion, was ligated with the synthesized primary sequence of miR-19b (Macrogen Inc.) to generate pRmiR-19b. Further, pRmiR-19b construct was digested with ClaI to take out the insert GFP-miR-19b. This insert was ligated with RCAS BP(A) construct (Petropoulos and Hughes, 1991) linearized with ClaI to obtain RCAS-miR-19b.

2. Sensor-ND1-WT: The chicken *Neurod1* 3'UTR having miR-19b target region with flanking NotI and HindIII sites were synthesized (Macrogen Inc.) and ligated in

pCAG-mCherry construct (a gift from Prof. Constance Cepko, Harvard Medical School, USA), downstream of the mCherry. Chicken *Neurod1* target region: (NM_204920.1 from 1380th nucleotide position to 1458th nucleotide position) 5'TACTACTTGTTACCTTTCCCGCGCCGAATTATTTTGTTGTGGTTTTGTACAG AATTTTTAATGACTTTTTATAACGTG3'.

3. Sensor-ND1-MUT**:** The above-mentioned strategy was used to generate this construct, by ligating a synthesized DNA fragment of *Neurod1* with mutated miR-19b target region (Macrogen Inc.) in the pCAG-mCherry construct. Chicken *Neurod1* mutated (in bold letters) target region: 5'TACTACTTGTTACCTTTCCCGCGCCGAATTATTTTGTTGTGGTTT**ACTT**CAG AATTTTTAATGACTTTTTATAACGTG3'

4. pSponge-19b and RCAS-Sponge-19b: For this first three copies of miR-19b target sequence (written in bold letters) was ligated in the pRmiR vector (Smith et al., 2009) to obtain pSponge-19b-3x construct 5'TGCTGCCGt**cagttttgcacctttgcaca**CCGG**tcagttttgcacctttgcaca**CCGG**tcagttttgcacctttgcaca**CCGG3'

   Then, using SalI, BglII, and BamHI Sponge-19b-3X sequence was chained in tandem to obtain twelve copies of sponge-19b and this construct was named pSponge-19b (Ebert and Sharp, 2010).

Testing the efficacy of Sponge-19b constructs:

To test the efficacy of Sponge-19b construct, HEK-293T cells were co-transfected with DNA constructs mentioned below in the following combination in separate dishes: i) pRmiR-Empty and Sensor-ND1-WT at 6:1 molar ratio, ii) pRmiR-Empty: pRmiR-19b: Sensor-ND1-WT at 3:3:1 molar ratio and iii) pRmiR-19b: Sponge-19b: Sensor-ND1-WT at 3:3:1 molar ratio. We found that the repression of mCherry from the construct, Sensor-ND1-WT imparted by expression of miR-19b from pRmiR-19b construct, was rescued by co-expression of Sponge-19b with miR-19b (pRmiR-Empty with Sensor-ND1-WT: 25.39 ± 0.17 A.U., pRmiR-Empty and pRmiR-19b with Sensor-ND1-WT: 17.61 ± 0.18 A.U., pSponge-19b and pRmiR-19b with Sensor-ND1-WT: 30.76 ± 0.12 A.U.; Fig. S4C to K and L). This indicated that Sponge-19b most likely sequesters miR-19b which results in loss-of-function of miR-19b.

5. pCAG-ND1-DBD_EnR: This construct was cloned by first amplifying chicken *Neurod1* DNA binding domain by Phusion Polymerase using the following primers (Forward Primer: 5'TTAGAAGACCCCATGACCAAGTCGTACAGC3' and Reverse Primer: 5'AGATGAATTCGAGCGCGGCGCCGTAGGCGT3') and then ligated in the NcoI and EcoRI digested pSlax-EnR vector (gifted by Prof. Andrew Lassar, Harvard Medical School, USA) to obtain pSlax-ND1-DBD_EnR. Finally, this ND1-DBD_EnR fragment was excised out and ligated at the same site in pCAG-MCS vector at the same site to obtained pCAG-ND1-DBD_EnR construct.

6. pCAG-GFP was a gift from Prof. C. Cepko, Harvard Medical School, USA.

Sensor assay

HEK-293T cells were transfected using Turbofect (Thermo Fisher Scientific Inc., R0533) as per manufacturer's protocol, with pRmiR vector(s) and respective Sensor vector(s) following which GFP and mCherry fluorescence were observed after 72 hours.

***In ovo* electroporation**

Fertilized chicken eggs were incubated overnight and lowered by taking out 2-3ml of albumin. Then, a window cut in the shell on the top and into one of the forebrain vesicles the DNA construct (2µg/µl) with 0.1% of fast green (Sigma-Aldrich, 44715) was injected. Platinum hockey stick electrodes (Nepagene, Japan) were used to deliver an electric current of 13V in five pulses for 50ms duration with a gap of 950ms, to the HH22 chick embryo head, using an electroporator (ECM830 Harvard instruments, USA). Then, before sealing with the tape, Penicillin, and Streptomycin with sterile PBS, was added over the embryos. Finally, harvesting was done at the desired HH stage.

Immunofluorescence staining

Briefly, after 4% PFA fixation for 5 minutes, three PBT washes were performed. Blocking was performed with 5% of heat-inactivated goat serum (HINGS) for 1 hour. Primary antibody was added and incubated overnight at 4˚C. The primary antibodies were used at the following dilution: anti-*Neurod1*, 1:1500 (Abcam, ab60704), anti-pH3, 1:300 (Sigma, H0412). After washing three times in PBT for five minutes each, the

appropriate secondary antibody was added. Secondary antibodies were as follows: Alexa Flour 594-conjugated Anti-Mouse IgG, 1:250 (Jackson ImmunoResearch Laboratories, INC., 115-585-003) and Alexa Flour 594-conjugated Anti-Rabbit IgG, 1:250 (Jackson ImmunoResearch Laboratories, INC., 111-585-045).

Imaging

To obtain the images of RNA *in situ* hybridization as well as immunofluorescence a Leica stereomicroscope (DM500B) equipped with a DFC500 camera was used. Other fluorescent images were obtained using the multi-photon laser scanning confocal microscope LSM780 (Carl Zeiss Inc.) and ZEN 2011 software.

Statistical Analysis

Each set of experiments was repeated at least three times; for animals, n=1 means on one animal experiment was performed; for cell culture, n=1 means in one dish experiment was performed. Only samples with GFP and/or mCherry expression after transfection or electroporation were included in the analysis. ImageJ software was used to measure the fluorescence intensity during the sensor assay. Origin Pro 9.1 and Graph Pad Prism 7.0 were used to plot the graph and to perform unpaired student's t-test and calculate the significance.

Acknowledgments

We acknowledge Prof. Amitabha Bandhopadhyay (Indian Institute of Technology Kanpur, India) for giving valuable suggestions for designing experiments as well as for critical comments on the manuscript. We are grateful to Ms Neetu Dey (Advanced Centre

for Material Sciences, Indian Institute of Technology Kanpur, India) for helping with confocal imaging.

Funding

This work was supported by a grant from Science and Engineering Research Board, Department of Science & Technology, Govt. of India. (EMR/2016/000886) to J.S. Council of Scientific and Industrial Research, Govt. of India supported S.K.S. for his Ph.D. fellowship (09/092(0824)/2011-EMR-I). A.M. and N.U. are supported by Ministry of Human Resources and Development, Govt. of India, for their fellowships.

Author contributions

Conceptualization S.K.S., and J.S.; Methodology, S.K.S., A.M., N.U. and J.S.; Investigation and Analysis, S.K.S., A.M., N.U., and J.S.; Writing, S.K.S., A.M., N.U., and J.S.; Funding Acquisition, J.S.

Competing interests

None declared.

REFERENCES

Agarwal, V., Bell, G. W., Nam, J. W. and Bartel, D. P. (2015). Predicting effective microRNA target sites in mammalian mRNAs. *Elife* **4**, 1–38.

Bian, S., Hong, J., Li, Q., Schebelle, L., Pollock, A., Knauss, J. L., Garg, V. and Sun, T. (2013). MicroRNA Cluster miR-17-92 Regulates Neural Stem Cell Expansion and Transition to Intermediate Progenitors in the Developing Mouse Neocortex. *Cell Rep.* **3**, 1398–1406.

Briscoe, S. D., Albertin, C. B., Rowell, J. J. and Ragsdale, C. W. (2018). Neocortical Association Cell Types in the Forebrain of Birds and Alligators. *Curr. Biol.* **28**, 686–696.e6.

Dugas-Ford, J., Rowell, J. J. and Ragsdale, C. W. (2012). Cell-type homologies and the origins of the neocortex. *Proc. Natl. Acad. Sci.* **109**, 16974–16979.

Ebert, M. S. and Sharp, P. A. (2010). MicroRNA sponges: Progress and possibilities. *RNA* **16**, 2043–2050.

Gupta, S., Maurya, R., Saxena, M. and Sen, J. (2012). Defining structural homology between the mammalian and avian hippocampus through conserved gene expression patterns observed in the chick embryo. *Dev. Biol.* **366**, 125–141.

Hamburger, V. and Hamilton, H. L. (1951). A series of normal stages in the development of the chick embryo. *Dev. Dyn.* **88**, 49–92.

Kawakami, A., Kimura-Kawakami, M., Nomura, T. and Fujisawa, H. (1997). Distributions of PAX6 and PAX7 proteins suggest their involvement in both early and late phases of chick brain development. *Mech. Dev.* **66**, 119–130.

Lee, J. E., Hollenberg, S. M., Snider, L., Turner, D. L., Lipnick, N. and Weintraub, H.

(1995). Conversion of Xenopus ectoderm into neurons by NeuroD, a basic helix-loop-helix protein. *Science* **268**, 836–44.

Pataskar, A., Jung, J., Smialowski, P., Noack, F., Calegari, F., Straub, T. and Tiwari, V. K. (2016). NeuroD1 reprograms chromatin and transcription factor landscapes to induce the neuronal program. *EMBO J.* **35**, 24–45.

Petropoulos, C. J. and Hughes, S. H. (1991). (1991). Replication-competent retrovirus vectors for the transfer and expression of gene cassettes in avian cells. *J. Virol.* 65, 3728-3737.

Sindhu, S. K., Udaykumar, N., Ali, M., Zaidi, A., Soni, A. and Sen, J. (2019). MicroRNA-19b restricts Wnt7b to the hem , which induces aspects of hippocampus development in the avian forebrain. *Development* **146**, dev175729.

Smith, C. A., Roeszler, K. N., Ohnesorg, T., Cummins, D. M., Farlie, P. G., Doran, T. J. and Sinclair, A. H. (2009). The avian Z-linked gene DMRT1 is required for male sex determination in the chicken. *Nature* **461**, 267–271.

Stark, A., Brennecke, J., Bushati, N., Russell, R. B. and Cohen, S. M. (2005). Animal microRNAs confer robustness to gene expression and have a significant impact on 3'UTR evolution. *Cell* **123**, 1133–1146.

Suzuki, I. K., Kawasaki, T., Gojobori, T. and Hirata, T. (2012). The Temporal Sequence of the Mammalian Neocortical Neurogenetic Program Drives Mediolateral Pattern in the Chick Pallium. *Dev. Cell* **22**, 863–870.

Thompson, R. C., Deo, M. and Turner, D. L. (2007). Analysis of microRNA expression by in situ hybridization with RNA oligonucleotide probes. *Methods* **43**, 153–61.

Trimarchi, J. M., Stadler, M. B., Roska, B., Billings, N., Sun, B., Bartch, B. and Cepko, C. L. (2007). Molecular heterogeneity of developing retinal ganglion and

amacrine cells revealed through single cell gene expression profiling. *J. Comp. Neurol.* **502**, 1047–1065.

Yamashita, W., Takahashi, M., Kikkawa, T., Gotoh, H., Osumi, N. and Ono, K. (2018). Conserved and divergent functions of Pax6 underlie species- specific neurogenic patterns in the developing amniote brain. *Development* **145**, dev159764

Yan, R. T. and Wang, S. Z. (2004). Requirement of NeuroD for Photoreceptor Formation in the Chick Retina. *Investig. Ophthalmol. Vis. Sci.* **45**, 48–58.

Zhang, Z. W., Zhang, L. Q., Ding, L., Wang, F., Sun, Y. J., An, Y., Zhao, Y., Li, Y. H. and Teng, C. B. (2011). MicroRNA-19b downregulates insulin 1 through targeting transcription factor NeuroD1. *FEBS Lett.* **585**, 2592–2598.

Fig. 1. Expression analysis of miR-19b, PH3 positive cells, and *Neurod1in the embryonic chick pallium*. (I-III) Schematic of a coronal section at the middle plane of HH24, HH29, and HH35 chick embryo forebrain. VZ, ventricular zone; SVZ, sub-ventricular zone; D, dorsal; V, ventral. (A, E, and I) Expression of miR-19b detected by *in situ* hybridization in the forebrain at HH24, HH29, and HH35, pseudo-colored in green. (B, F, and J) Expression of *Neurod1* detected by immune-staining on the same section of (A, E, and I). (C, G, and K) Analysis of PH3 positive cells on the adjacent sections of (A, E, and I). (D, H, and L) Merged images of miR-19b and *Neurod1* expression analysis (A, E, and I), and (B, F, and J). (A'-D') High magnification view of the white-dash boxed region of (A-D). (E'-H'), and (I'-L') High magnification view of the pink-dash boxed region of (E-H), and (I-L). (E''-H''), and (I''-L'') High magnification view of the yellow-dash boxed region of (E-H), and (I-L). White-arrows indicating the extent of expression domain. (E'*, E''*, I'*, and I''*) Star '*' mark region representing the white-dashed boxed region in (E', E'', I', and I'') showing the expression of miR-19b in the ventricular zone regions of respective images. (M) Schematic to summarize expression analysis of miR-19b, *Neurod1*, and PH3 positive cells in chick pallium at HH24, HH29, and HH35. Scale bar: (A-H) 500µm, (I-L) 800µm, (A'-L'), and (E''-L'') 250µm, (E'*, E''*, I'*, and I''*) 50µm.

Fig. 2. The effect of miR-19b expression on cell proliferation in the developing chick forebrain. (A) Schematics of DNA constructs used for manipulation of expression of miR-19b. (B) Schematic of *in ovo* electroporation at HH22 followed by harvesting and analysis of brains at HH34. High magnification view of the blue-boxed region shown in (C-E). D, dorsal; V, ventral; VZ, ventricular zone; SVZ, sub-ventricular zone. (C) RCAS-GFP (n=6), (D) RCAS-miR-19b (n=6), and (E) RCAS-Sponge-19b (n=6) electroporation in the chick forebrain sections indicated by of GFP-positive cells in green on which PH3-positive proliferating cells are indicated in red color. (C'-E') PH3-positive cells in the ventricular zone (VZ) of (C-E), among which PH3-GFP double-positive cells are indicated by yellow arrowheads and only PH3-positive cells are indicated by white-arrowheads. (F) Quantification of the percentage of GFP-positive cells that also are PH3-positive analyzed in (C-E). Data: Mean ± S.E.M., Scale bar represents 50μm. ** $P \leq 0.01$, ***$P \leq 0.001$.

Fig. 3. Effect of gain-of-function of miR-19b on the expression of *Neurod1*. (A) Schematics of the DNA constructs used, RCAS-GFP and RCAS-miR-19b. (B) Schematic showing microinjection and electroporation of the respective DNA constructs performed at HH22 followed by harvesting and analysis of the coronal section of the forebrain at HH34. VZ, ventricular zone; SVZ, sub-ventricular zone; D, dorsal; V, ventral. (C, F) GFP expression from RCAS-GFP (n=4) and RCAS-miR-19b (n=4) electroporated regions indicated by green color. (D, G) *Neurod1* immuno-staining indicated in red color in RCAS-GFP and RCAS-miR-19b electroporated forebrain sections. (E, H) Merged images of (C, F) and (D, G). (I) Quantification of the percentage of GFP-positive cells that are double-positive for GFP and *Neurod1* in the SVZ region. White arrows in the inset in (E, H) indicate GFP-*Neurod1* double-positive cells. T-test was performed, Data represents Mean $\pm$ S.E.M., ** $p \leq 0.01$, Scale bar: (C-H) 50µm.

Fig. 4. Effect of misexpression of miR-19b and expression of the dominant-negative form of *Neurod1* on *Mef2c* expression in the chick pallium. (A) Schematics of DNA constructs used for manipulation of expression of miR-19b and *Neurod1*. (B) Schematic of HH22 chick embryo forebrain, in which microinjection and electroporation were performed to target the dorsolateral mesopallium region followed by harvesting at HH29. D, dorsal; V, ventral. High magnification view of the black-boxed region is shown in (C-K). (C, F, I) GFP expression in green color indicates the cells electroporated with pRmiR-Empty (n=3), pRmiR-19b (n=4) and pCAG-GFP & pCAG-ND-DBD_EnR (n=3). (D, G, J) *Mef2c* expression domain detected by mRNA in situ hybridization on the same sections of (C, F, I). (E, H, K) Merged images of (C, F, I) with (D, G, J) pseudo-colored in red. The region enclosed by dotted-line showing GFP expressing region and the region showing loss of *Mef2c* expression in the respective image (F-K) and unchanged expression of *Mef2c* in the control (C-E). Scale bar: (C-K) 100µm.

Fig. 1

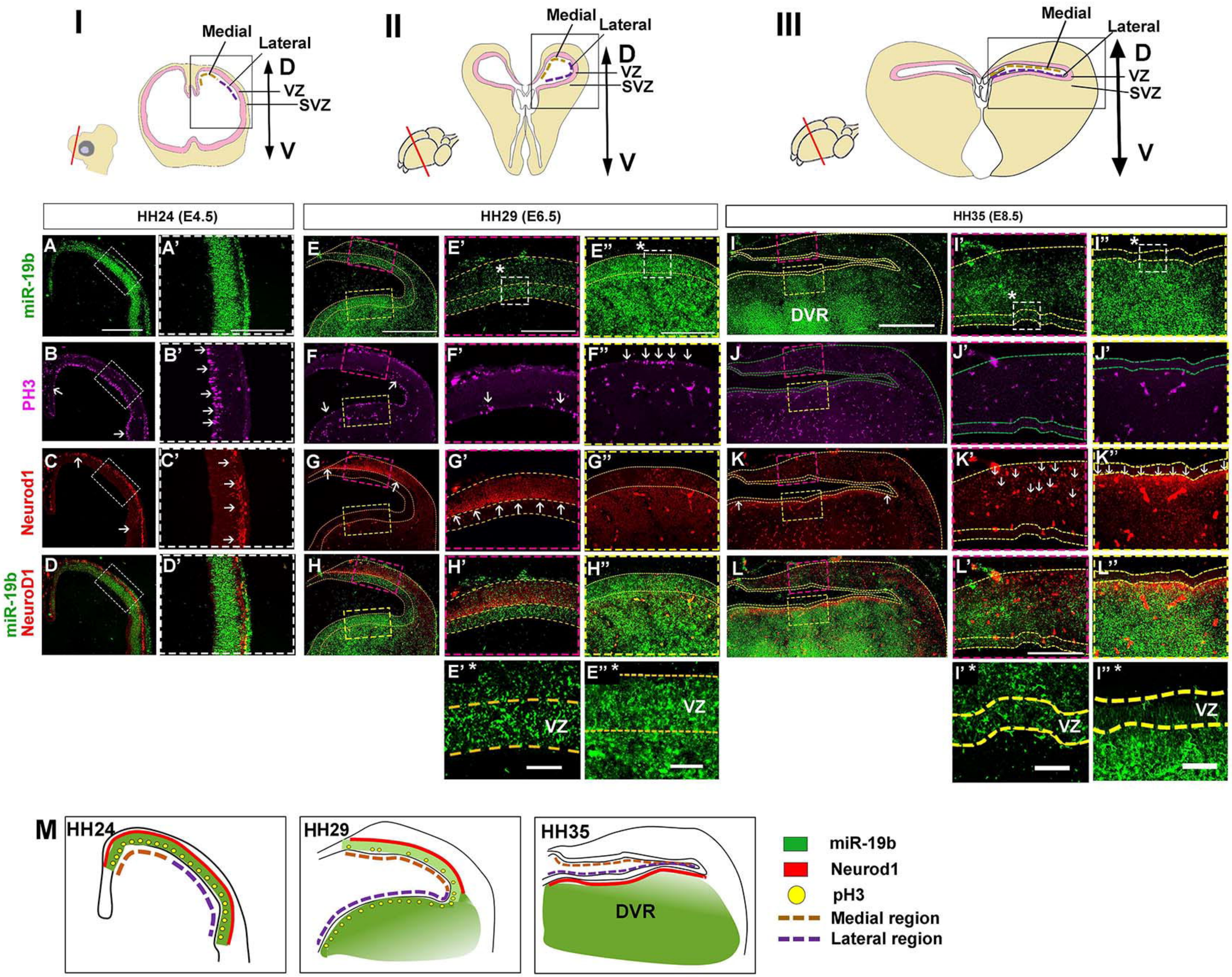
I
Medial
Lateral
D
VZ
SVZ
V
II
Medial
Lateral
D
VZ
SVZ
V
III
Medial
Lateral
D
VZ
SVZ
V
HH24 (E4.5)
HH29 (E6.5)
HH35 (E8.5)
miR-19b
PH3
Neurod1
miR-19b
NeuroD1
DVR
VZ
M
HH24
HH29
HH35
DVR
miR-19b
Neurod1
pH3
Medial region
Lateral region

Fig. 2

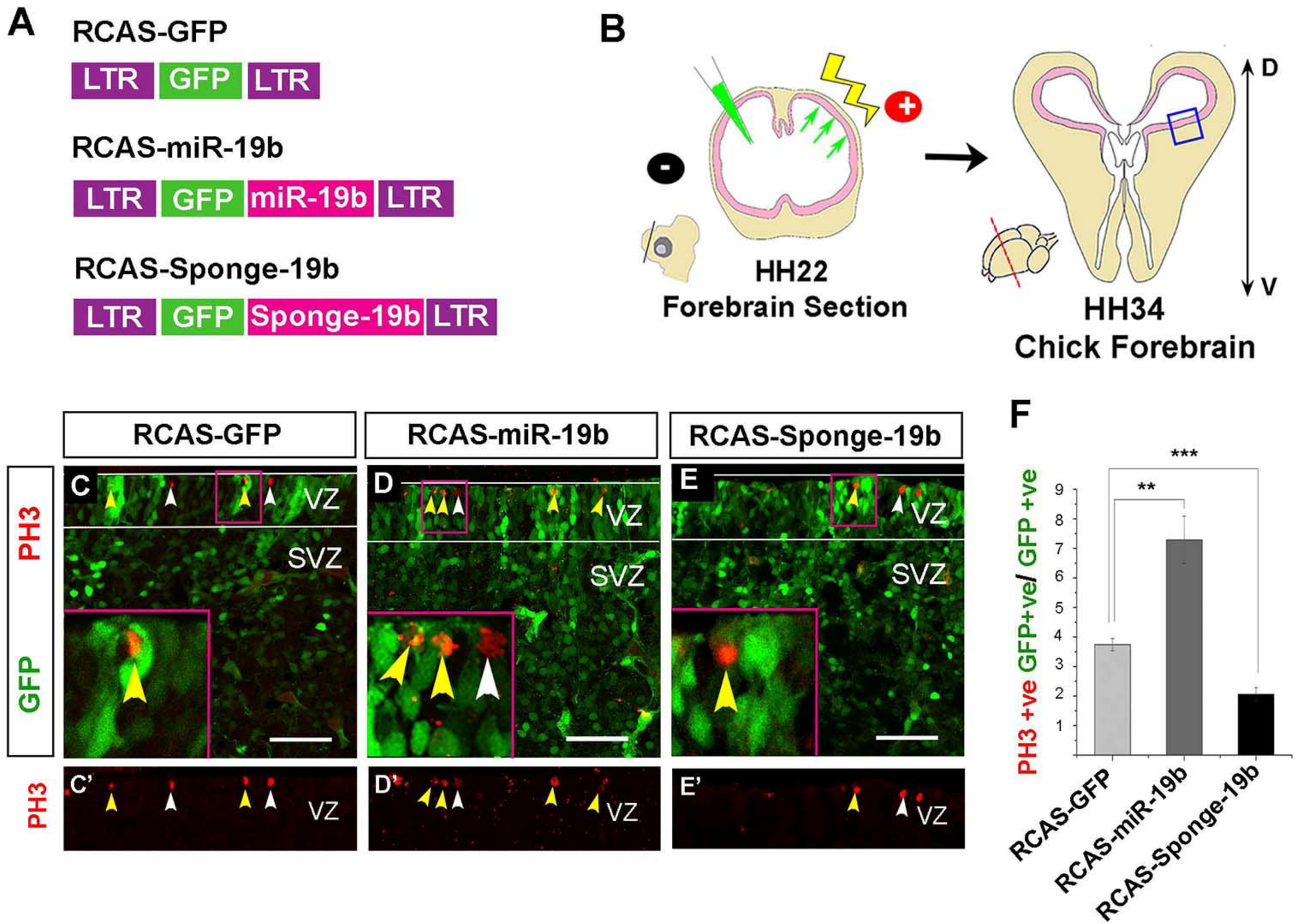
A
RCAS-GFP
LTR GFP LTR
RCAS-miR-19b
LTR GFP miR-19b LTR
RCAS-Sponge-19b
LTR GFP Sponge-19b LTR
B
HH22
Forebrain Section
HH34
Chick Forebrain
D
V
RCAS-GFP
RCAS-miR-19b
RCAS-Sponge-19b
PH3
GFP
C
D
E
VZ
SVZ
C'
D'
E'
F
PH3 +ve GFP+ve/ GFP +ve
***
**
RCAS-GFP
RCAS-miR-19b
RCAS-Sponge-19b

Fig. 3

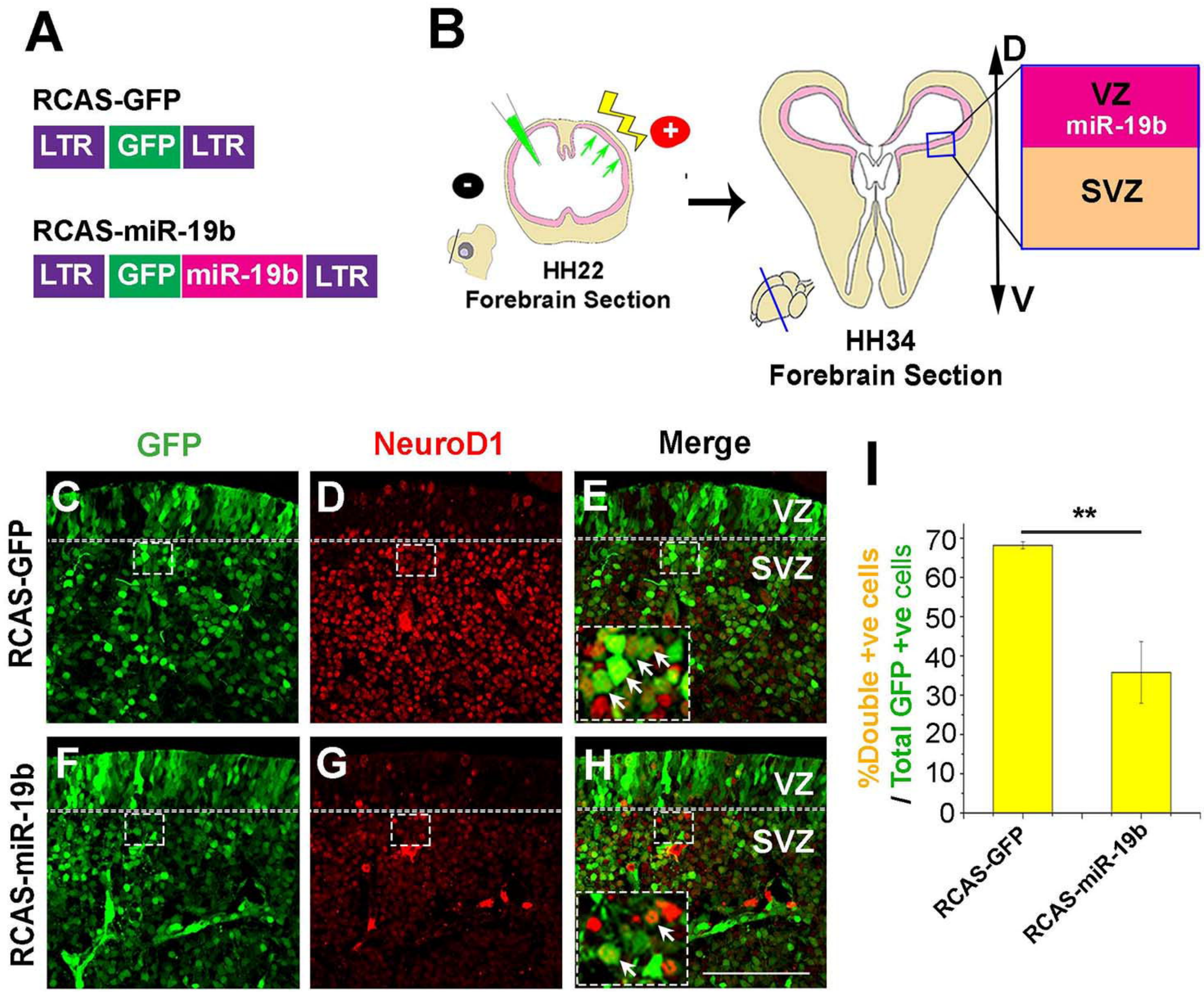
A
RCAS-GFP
LTR GFP LTR
RCAS-miR-19b
LTR GFP miR-19b LTR
B
HH22
Forebrain Section
HH34
Forebrain Section
D
V
VZ
miR-19b
SVZ
GFP
NeuroD1
Merge
RCAS-GFP
RCAS-miR-19b
C
D
E
F
G
H
VZ
SVZ
I
**
%Double +ve cells
/ Total GFP +ve cells
70
60
50
40
30
20
10
0
RCAS-GFP
RCAS-miR-19b

Fig. 4

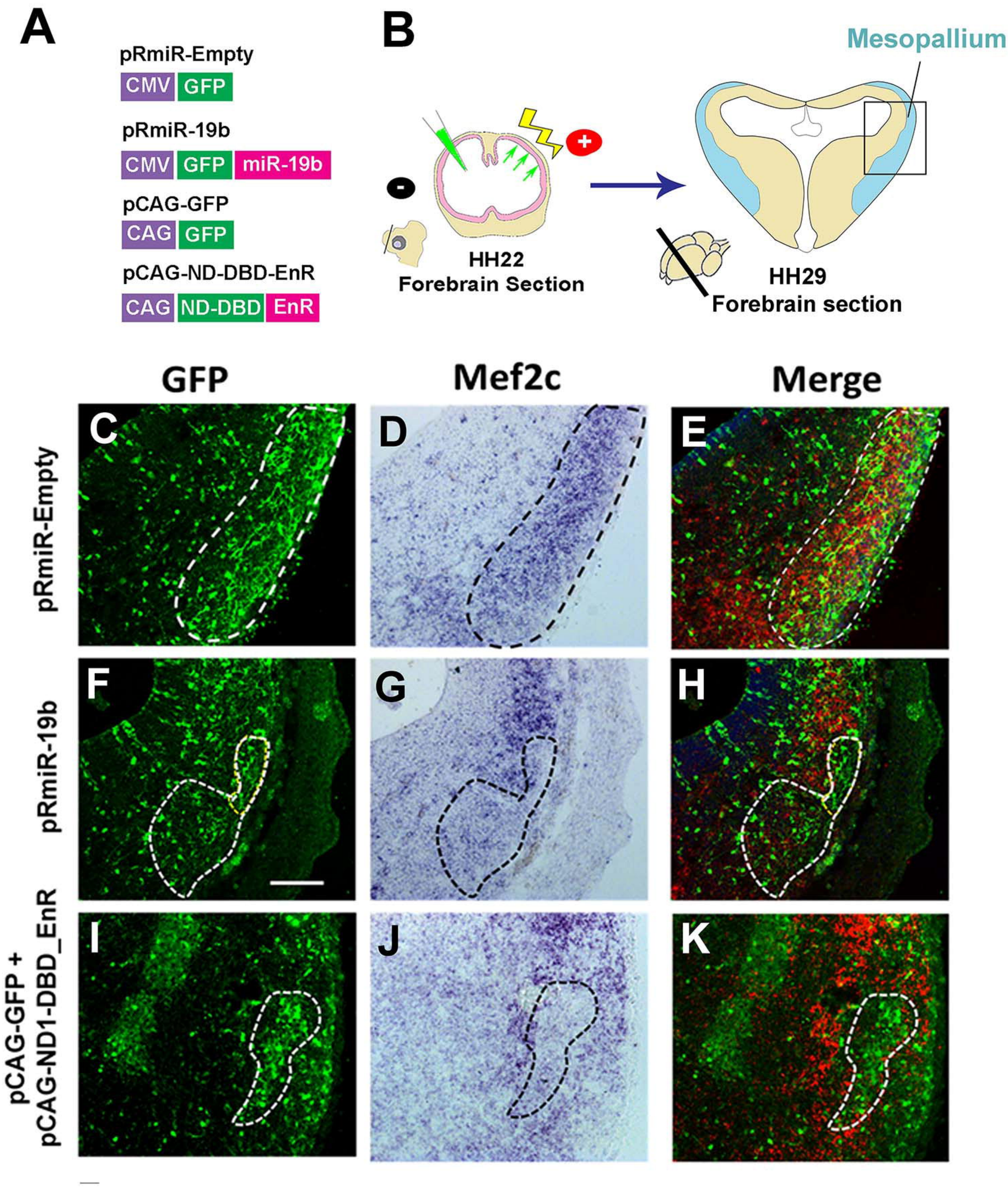
A
pRmiR-Empty
CMV
GFP
pRmiR-19b
CMV
GFP
miR-19b
pCAG-GFP
CAG
GFP
pCAG-ND-DBD-EnR
CAG
ND-DBD
EnR
B
Mesopallium
HH22
Forebrain Section
HH29
Forebrain section
GFP
Mef2c
Merge
C
D
E
F
G
H
I
J
K
pRmiR-Empty
pRmiR-19b
pCAG-GFP +
pCAG-ND1-DBD_EnR